UNCLASSIFIED

AD NUMBER
AD840352
LIMITATION CHANGES

TO:

Approved for public release; distribution is unlimited.

FROM:

Distribution authorized to U.S. Gov't. agencies and their contractors; Critical Technology; SEP 1968. Other requests shall be referred to Air Force Weapons Laboratory, Kirtland AFB, NM. This document contains export-controlled technical data.

AUTHORITY
AFWL ltr, 30 Nov 1971

THIS PAGE IS UNCLASSIFIED

AD840352

STUDIES AND EXPERIMENTAL WORK ON

ATOMIC COLLISION PROCESSES OCCURRING

IN ATMOSPHERIC GASES

A. V. Phelps

W. H. Kasner

Westinghouse Research Laboratories

Pittsburgh, Pennsylvania

Contract F2960167C-0046

TECHNICAL REPORT NO. AFWL-TR-68-55

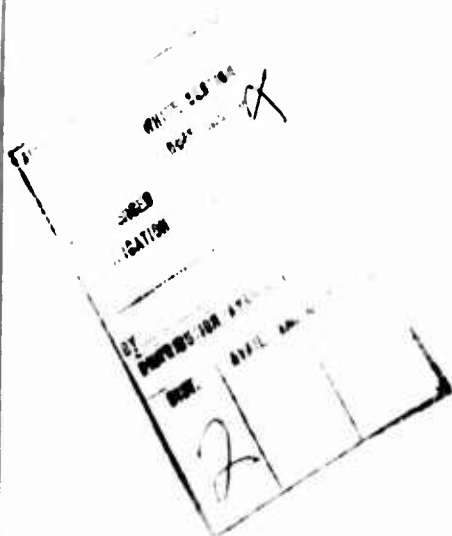September 1968

AIR FORCE WEAPONS LABORATORY

Air Force Systems Command

Kirtland Air Force Base

New Mexico

47

AIR FORCE WEAPONS LABORATORY
Air Force Systems Command
Kirtland Air Force Base
New Mexico

AFWL-TR-68-55

STUDIES AND EXPERIMENTAL WORK ON ATOMIC COLLISION

PROCESSES OCCURRING IN ATMOSPHERIC GASES

A. V. Phelps

W. H. Kasner

Westinghouse Research Laboratories
Pittsburgh, Pennsylvania
Contract F2960167C-0046

TECHNICAL REPORT NO. AFWL-TR-68-55

FOREWORD

This report was prepared by Westinghouse Research Laboratories, Pittsburgh, Pennsylvania, under Contract F2960167C-0046. The research was performed under Program Element 61102H, Project 5710, Subtask 07.011.5710-5710U-815, MIPR 529-67, and was funded by the Defense Atomic Support Agency (DASA).

Inclusive dates of research were 20 February 1967 to 21 February 1968. The report was submitted 5 August 1968 by the AFWL Project Officer, Capt Joseph S. Greene, Jr. (WLRT).

The work discussed in the various sections of this report was carried out by the following personnel: Section II, J. L. Moruzzi and A. V. Phelps; Section III, W. H. Kasner.

This report has been reviewed and is approved.

JOSEPH S. GREENE, JR.
Captain, USAF
Project Officer

TRUMAN L. FRANKLIN
Colonel, USAF
Chief, Theoretical Branch

CLAUDE K. STAMBAUGH
Colonel, USAF
Chief, Research Division

ABSTRACT

The rate coefficients for electron attachment to ozone have been measured in N_2-O_3 mixtures and are found to increase from 8×10^{-12} to 1.8×10^{-10} cm^3/sec as the characteristic electron energy increases from 0.1 and 0.8 eV. The dependence of the attachment rate coefficient on the ozone pressure at electron energies near 0.15 eV is consistent with a two-body attachment process, presumably dissociative attachment. The temperature dependence of the recombination coefficient for electrons and O_2^+ can be approximated by T_{gas}^{-1} with the actual values being $(3.0 \pm 0.3) \times 10^{-7}$ cm^3/sec at 205°K, $(2.2 \pm 0.2) \times 10^{-7}$ cm^3/sec at 295°K, and $(1.0 \pm 0.2) \times 10^{-7}$ cm^3/sec at 690°K. The recombination coefficient for electrons and O_4^+ at 205°K is estimated to be 2.3×10^{-6} cm^3/sec.

Distribution Limitation Statement No. 2

(This page was intentionally left blank)

CONTENTS

ILLUSTRATIONS

vii

(This page was intentionally left blank)

STUDIES AND EXPERIMENTAL WORK ON ATOMIC
COLLISION PROCESSES OCCURRING IN ATMOSPHERIC GASES

SECTION I

SUMMARY

This technical report describes: a) a preliminary experimental investigation of electron attachment and detachment in ozone; and b) an experimental study of the temperature dependence of electron-positive ion recombination in atmospheric gases. The rate coefficients for these processes are needed for the prediction and analysis of the electrical behavior of the earth's atmosphere in the presence of natural and artifically induced ionization.

Conventional drift-tube techniques have been used to study the attachment and detachment of low-energy electrons to ozone. In these studies, the attachment rate coefficient is determined from the slope of the ion current waveform observed at the collector. Multichannel signal averaging techniques have been used to improve the signal to noise ratio of these ion current waveforms. Initial studies in pure ozone indicated very large attachment rates, and yielded ion waveforms that were difficult to analyze. To overcome this difficulty the ozone was diluted with nitrogen, a non attaching gas. By using estimated characteristic electron energies and electron drift velocities for the various N_2-O_3 gas mixtures, the attachment rate coefficients were determined for energies between 0.1 and 0.8 eV. At energies near 0.15 eV the concentration of O_3 in the mixtures was varied from 0.5 to 3.5 Torr for total pressures of 50 Torr. The results are consistent with a two-body attachment process, presumably dissociative attachment. The attachment rate coefficients vary from 8×10^{-12} to 1.8×10^{-10} cm^3/sec as the characteristic energy varies from 0.1 to 0.8 eV. These results must be regarded as preliminary because some of the waveforms at low electron energies show evidence of electron detachment.

The temperature dependence of the coefficient for the recombination of electrons with mass identified O_2^+ ions has been determined from observations of the electron and ion decay rates in the afterglow following "single-pulse" microwave discharges in O_2-Ne, O_2-Ne-Ar, and O_2-Ne-Kr gas mixtures. In most cases, these studies were conducted under conditions where O_2^+ was the only significant afterglow ion species and where the recombination of electrons with the O_2^+ ions was the dominant loss mechanism. Temporal mass analysis, using multichannel signal averaging techniques, show similar decay rates for the electrons and for the O_2^+ ions over the major portion of the afterglow. The observed recombination coefficient, $\alpha(O_2^+)$, has a temperature dependence approximated by T_{gas}^{-1}, the actual values ranging from $(3.0 \pm 0.3) \times 10^{-7}$ cm^3/sec at 205°K to $(1.0 \pm 0.2) \times 10^{-7}$ cm^3/sec at 690°K. At lower temperatures (<250°K), the dimer ion $O_2 \cdot O_2^+$ becomes significantly more important. From an analysis of afterglow studies involving the simultaneous recombination of electrons with this dimer ion and with O_2^+ ions, we obtained an estimated value of $\alpha(O_2 \cdot O_2^+) = 2.3 \times 10^{-6}$ cm^3/sec at a gas temperature of 205°K.

SECTION II

ELECTRON ATTACHMENT AND DETACHMENT IN OZONE

1. Introduction

Analyses (Ref. 1) of the absorption of electromagnetic radiation at radar and radiometer frequencies following nuclear explosions in the upper atmosphere have indicated the presence of night-time electron removal processes that are faster than the well known three-body attachment to oxygen. These theoretical studies propose that the additional attachment is caused by dissociative attachment to ozone. Because the night-time ozone concentrations used in these analyses (Ref. 1) are highly uncertain, the derived attachment rate coefficient $(3 \times 10^{-13} \text{ cm}^3/\text{sec})$ is uncertain and must be measured in the laboratory. Additional interest in the effect of ozone on atmospheric deionization arises from the possibility of ion-molecule reactions such as charge transfer and associative detachment. Thus, Fehsenfeld, Schmeltekopf, Schiff, and Ferguson (Ref. 2) have found that O^- and O_2^- rapidly charge transfer to O_3 to form O_3^- and that O_3^- reacts with CO_2 to form CO_3^-. As we shall see below, there is evidence that one or more of these ions undergoes detachment in a reaction with ozone. The work described below represents the initial stages of a program designed to measure the rate coefficients for electron attachment and detachment and accompanying ion molecule reactions in O_3 and O_2-O_3 mixtures.

2. Apparatus

The experimental system (Figure 1) can be divided into two sections, a discharge region in which ozone is produced and trapped and a reaction region where the electron attachment properties of ozone can be studied. The ozone is produced by dissociating a flowing stream of oxygen gas. The discharge products pass through the cold trap, which freezes out the O_3, and then into the pumps through the bypass valve. A diatherm unit* is used to power the microwave cavity clamped around

---

*Raytheon Microtherm Model CMD4.

3
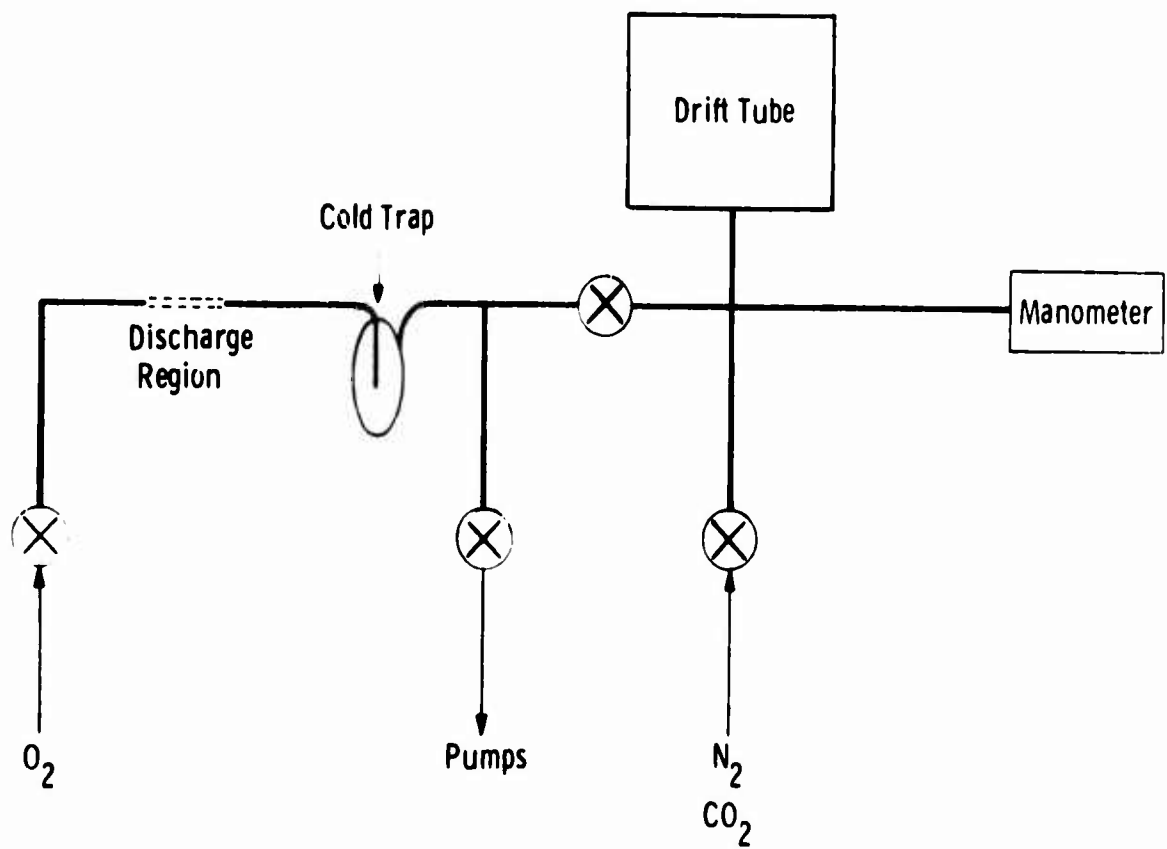
Fig. 1 - Ozone-gas-handling system.

the flow tube. The cold trap is maintained at liquid nitrogen tempera-
tures. The oxygen flow rate and the oxygen pressure are adjusted for
the maximum collection of ozone in the cold trap (Ref. 3). When
sufficient ozone, roughly 1/2 cc, has been collected, the discharge
is switched off, the oxygen flow stopped, and the trap is exposed to
the vacuum pumps for approximately one hour.

The reaction region of the apparatus consists of a uniform
field drift tube into which the ozone can be expanded. Provision is
also made to allow mixtures of ozone and nitrogen to be made. The
total pressure in the drift tube is measured by using a null-reading
diaphragm morometer (Ref. 4), which separates the vacuum system from
the oil manometer. The ozone density can be calculated from the
measured absorption of a known ultraviolet (uv) line. A low pressure
mercury lamp is used as a source and a Perkin Elmer monochromator is
used to select the desired line after it has passed through the drift
tube. Because the path length and the absorption coefficients for
ozone are known (Ref. 5), the ozone density in the drift region is
readily calculated. For ozone pressures between 0.01 and 0.5 Torr the
2536 $\overset{\circ}{A}$ Hg line is used, while higher ozone pressure can be measured by
using either the 2967 or the 3125 $\overset{\circ}{A}$ lines.

Because ozone is readily destroyed by metallic surfaces such
as Kovar, all the metal parts of the system, excluding the electrodes
of the drift tube, were coated with a thin Teflon film. The electrodes
were gold-plated discs and wires. With this arrangement the ozone
pressure change was less than 1 percent per minute.

The drift tube (Figure 2) consists of a semi-transparent
cathode (C) (Ref. 6), a set of guard rings, and a collector (S). A
short distance in front of the collector is a fine wire grid (G), which
shields the collector from induced currents caused by the movement of
charged particles across the drift region. By applying a suitable rf
voltage ($\approx$2MHz) to alternate grid wires, the grid can also serve as an
electron shutter (Ref. 7).

5
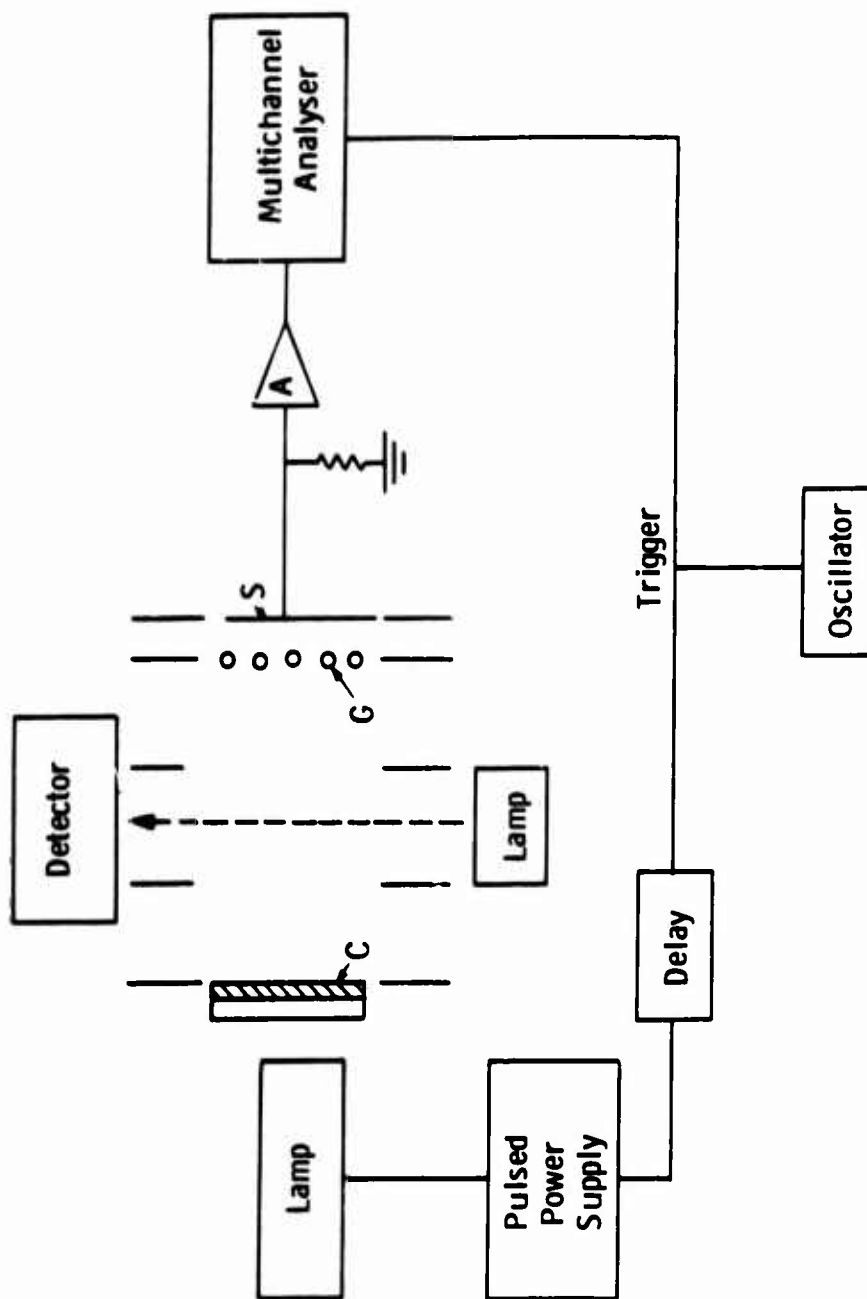
Fig. 2 - Apparatus for measurement of electron attachment and ozone density. The electrodes of the drift tube are enclosed in a stainless steel chamber fitted with uv windows and electrical feedthroughs.

6

As shown in Figure 2, a master oscillator triggers both the multichannel analyzer and the pulsed uv lamp, which releases electrons from the cathode. The lamp can be switched on for any selected time interval and the triggering of the lamp can be delayed relative to the start of the multichannel analyzer. Electrons are released from the cathode while the lamp is on and these electrons drift across the tube toward the collector under the influence of the applied electric field. The mean energy of these electrons is controlled by the nature of the gas in the gap and by the ratio E/p, where E is the electric field strength in $V\ cm^{-1}$ and p is the pressure in Torr. If no rf is applied to the grid wires, then the electrons reach the collector and cause a voltage to develop across the load resistor (R). This voltage is amplified and then digitized before being stored in the memory of the multichannel analyzer. If this procedure is repeated n times, then the signal to noise ratio (S/N) of the current waveform will improve by $\sqrt{n}$. In this manner, one can obtain S/N values comparable with those obtained by using synchronous detection schemes (Ref. 8 and 9) but in much less time.

If an attaching gas is present in the drift tube, some of the electrons released from the cathode will attach to form negative ions. Thus, the current waveform will have two components, a fast electron component and a slow ion component. When no rf is applied to the wire grid, the total current waveform will be collected, averaged, and recorded by the multichannel analyzer. An example of this mode of operation is shown in Figure 3. The upper trace indicates the duration of the light pulse, which is equal to the initial electron pulse width. The center trace is a "single shot" recording of the current waveform while the lowest trace is this same signal after it has been averaged 5000 times. This averaging process took approximately 2 min. Under the conditions of this experiment, the initial peak is caused by electrons that cross the gap without attaching while the remainder of the waveform is caused by negative ions formed by attachment.

7
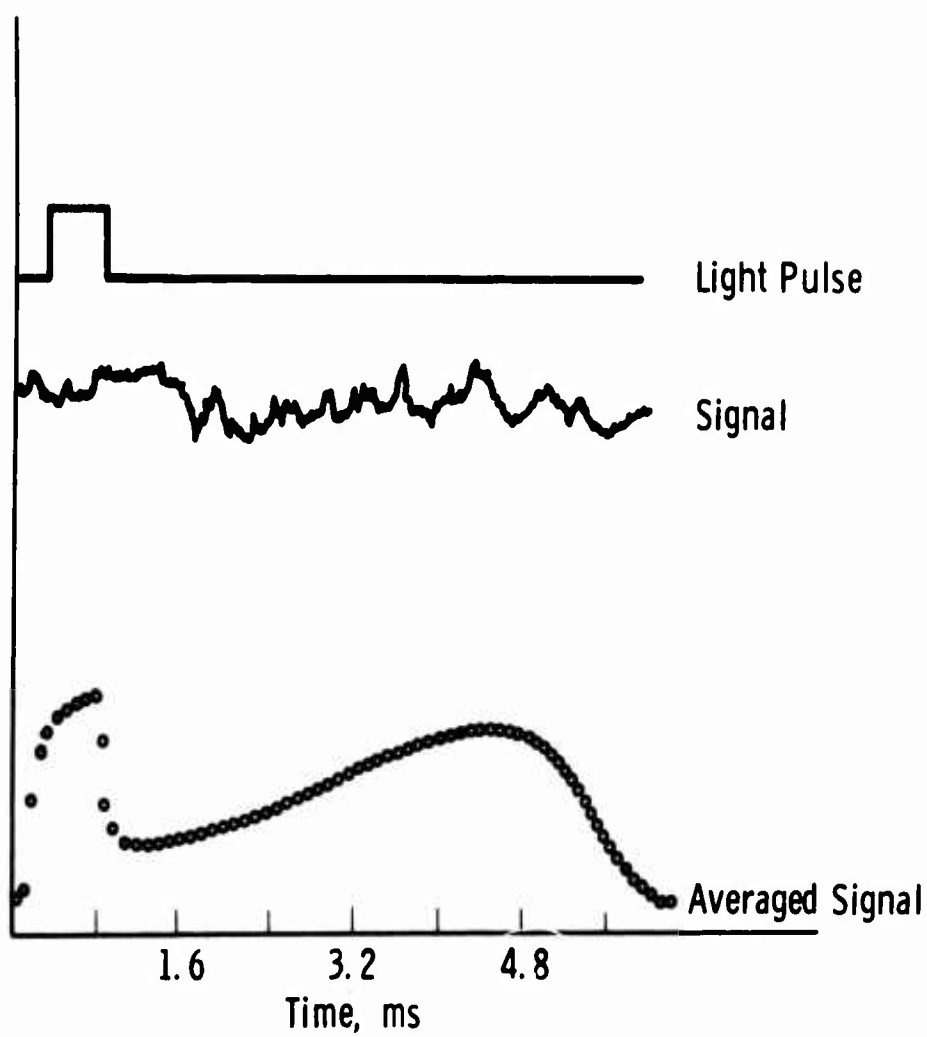
Fig. 3 - Typical waveforms for electron attachment measurements.

8

If the rf voltage is applied to the grid wires continuously, all electrons will be absorbed by the grid and the collected current will be the ion component of the waveform. However, if for one sweep no rf is applied and on the second sweep rf is applied, then the difference in the collected currents will give the electron component of the current waveform. Fortunately, this subtraction can be done internally in the multichannel analyzer. A schematic diagram of the circuitry necessary to perform this operation is shown in Figure 4. By using this technique, it is possible to obtain the total, the electron, and the ion current waveforms with adequate signal to noise.

3. Interpretation of Results

It has been shown by earlier work in this laboratory (Ref. 8) that for waveforms, such as that of Figure 3, it is possible to obtain the attachment rate coefficient either from the slope of the leading edge of the ion waveform or from the ratio of the areas under the total waveform and under the ion component of the waveform, provided the electron and ion drift velocities are known.

Preliminary investigations in oxygen at low E/p yielded values for the attachment coefficient in fair agreement, ±20%, with the data of Chanin, Phelps, and Biondi (Ref. 8). Our initial investigations with nominally pure ozone indicated such large attachment rates that all electrons attached close to the cathode, forming a narrow pulse of ions. Waveforms of this type cannot be analyzed in the manner described above. To overcome this problem, the ozone was diluted with nitrogen, a non-attaching gas. These mixtures were made by adding the required amount of nitrogen to a known amount of ozone already in the system. Figure 5 is an example of a total current waveform taken in such a mixture at $E/p_T = 0.112$ V cm^{-1} Torr^{-1}. The peak at early times is caused by unattached electrons crossing the tube, while the second peak is caused by the much slower negative ions that are formed throughout the drift space. It was found that the attachment coefficients, obtained by using either the "slope" or the "area" method, agreed to

9
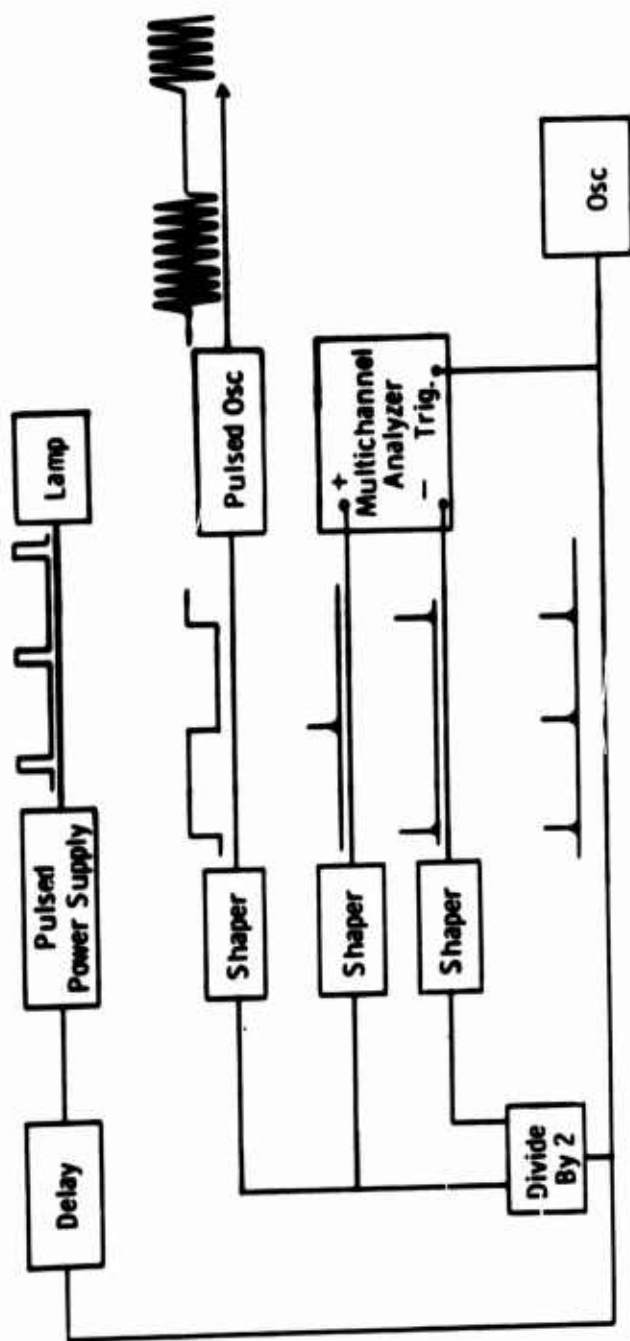
Fig.4 - Waveforms used to obtain electron component of current waveform. The mercury lamp pulse begins shortly after the trigger pulses and the beginning of the rf pulse.

10
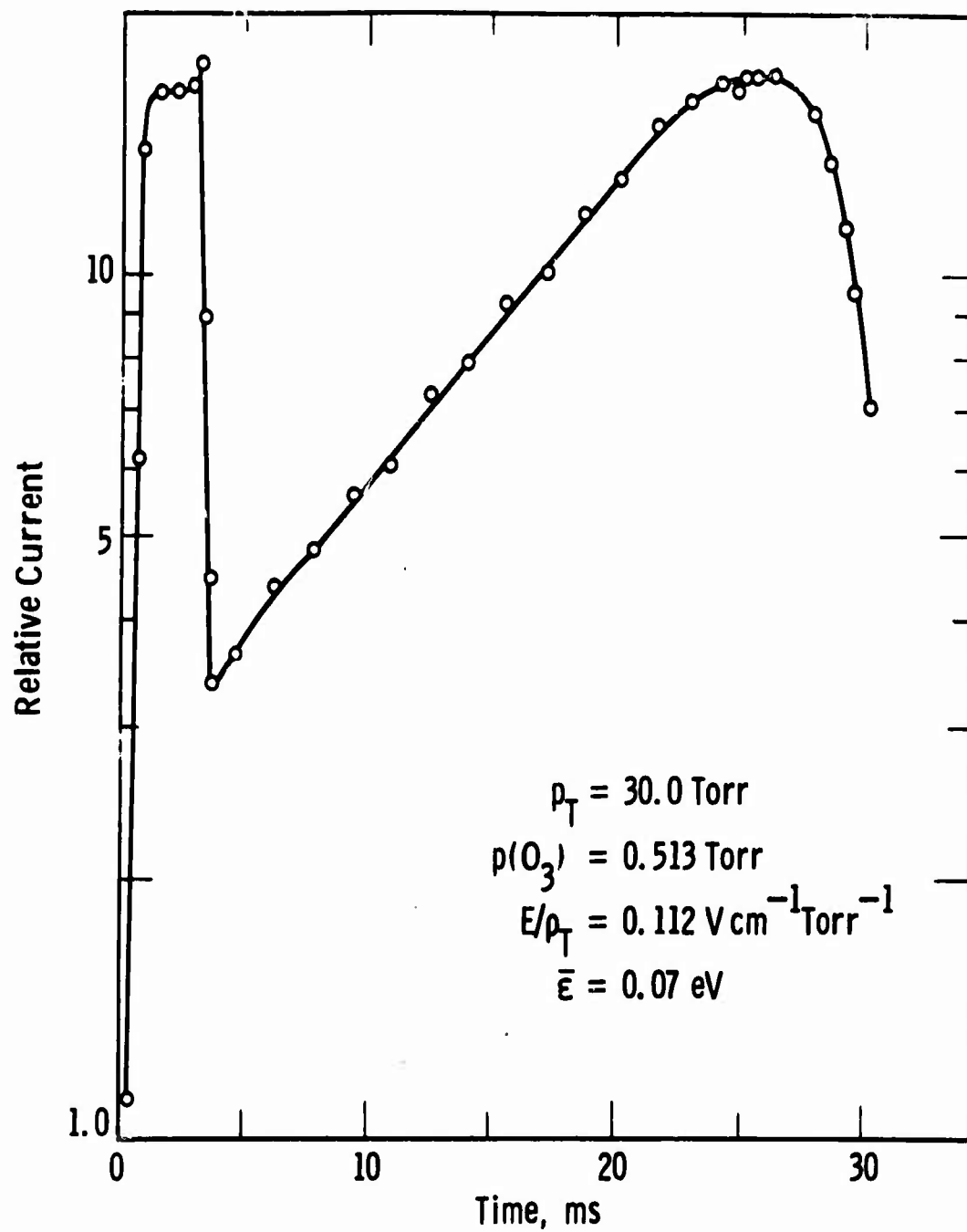
Fig. 5 – Total current waveform obtained under conditions suitable for good attachment coefficient determinations.

11

better than ±5 percent when the waveform showed a sharply decaying electron signal and an exponentially rising ion component as in Figure 5. By varying E/p_T the electron energy can be changed, and one is able to measure the attachment rate coefficient as a function of electron energy as given below.

The determination of the electron energy scale for electron energies below 0.3 eV presents some problems when the concentration of O_3 is above 0.2 percent because of a lack of information regarding elastic and inelastic scattering cross sections for electrons in O_3. We have estimated momentum transfer ν_m and energy exchange ν_u colli- sion frequencies for O_3 by using the known dipole moment of O_3. These quantities are related to the drift velocity, the characteristic energy, and E/N by (Ref. 10)

$$\nu_m/N = 1.758 \times 10^{15} \frac{E/N}{w} \tag{1}$$

and

$$\nu_u/N = \frac{w\ E/N}{\epsilon_k - kT}, \tag{2}$$

where N is the gas density, w is the electron drift velocity, ϵ_k is the characteristic electron energy and kT is the energy of the neutral gas. If the electron energy distribution were Maxwellian, the electron tempera- ture would be given by ϵ_k/k. The values of w, ϵ_k, and E/N for a gas mixture can be calculated if we assume that for the mixture,

$$\left.\frac{\nu_m}{N}\right|_{mixture} = \sum_i \left(\frac{\nu_m}{N}\right)_i \frac{N_i}{N} \tag{3}$$

and

$$\left.\frac{\nu_u}{N}\right|_{mixture} = \sum_i \left(\frac{\nu_u}{N}\right)_i \frac{N_i}{N}, \tag{4}$$

where N_i is the density of ith gas component. For the O_3-N_2 mixtures we have used the momentum transfer and energy loss frequencies given

12

by Engelhardt, Phelps, Risk (Ref. 11) for nitrogen and estimates for ozone. By using these assumptions, the characteristic electron energy and electron drift velocity for any mixture of O_3-N_2 can be calculated as a function of E/p_T applied to the mixture. Obviously, there is a need for definitive measurements of electron transport coefficients in O_3 and mixtures of ozone with other gases.

For ozone pressures greater than 0.2 Torr, the electron and ion waveforms show a clear separation of the electron and ion components as in Figure 5. However, at lower ozone pressures there is evidence of delayed currents because of detached electrons. An example of this is shown in Figure 6 where the upper waveform is the electron current observed in pure nitrogen at 24 Torr. Because no attachment occurs in nitrogen, this waveform is almost identical to the pulse of electrons leaving the cathode and clearly establishes the response of the detection system and the cut-off time of the lamp. The lower two curves are the electron and ion components of the total waveform after 0.018 Torr of ozone had been added to the system. The electron curve clearly indicates the presence of delayed electron currents, which we interpret as resulting from a detachment reaction. The lower curve is the waveform caused by negative ions. The presence of a negative ion current at the collector after the source of detached electrons has disappeared is most readily explained by proposing the presence of a second ion that is stable against detachment.

4. Attachment Data

The data presented in Figure 7 are a summary of the attachment rate coefficients obtained in various O_3-N_2 mixtures for characteristic electron energies between 0.035 and 0.9 eV. The mixture pressures ranged between 10 and 60 Torr and contained between 0.5 and 16 percent ozone. It should be emphasized that these data are taken from waveforms where detachment effects were small. Over the ozone pressure range investigated, it can be seen that all the points fall within a reasonably narrow band. This is consistent with a two-body
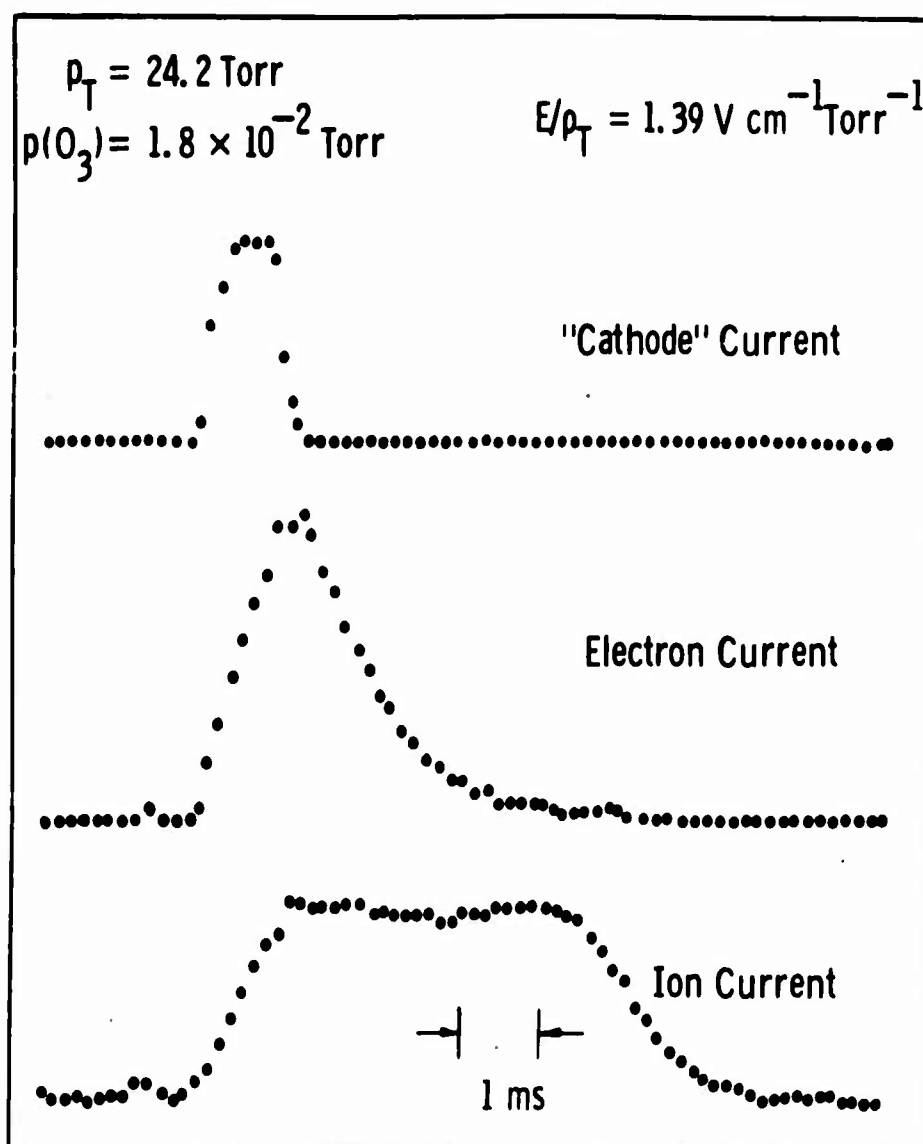
Fig. 6 - Electron and ion current waveforms showing apparent electron detachment at low O_3 concentrations.

14
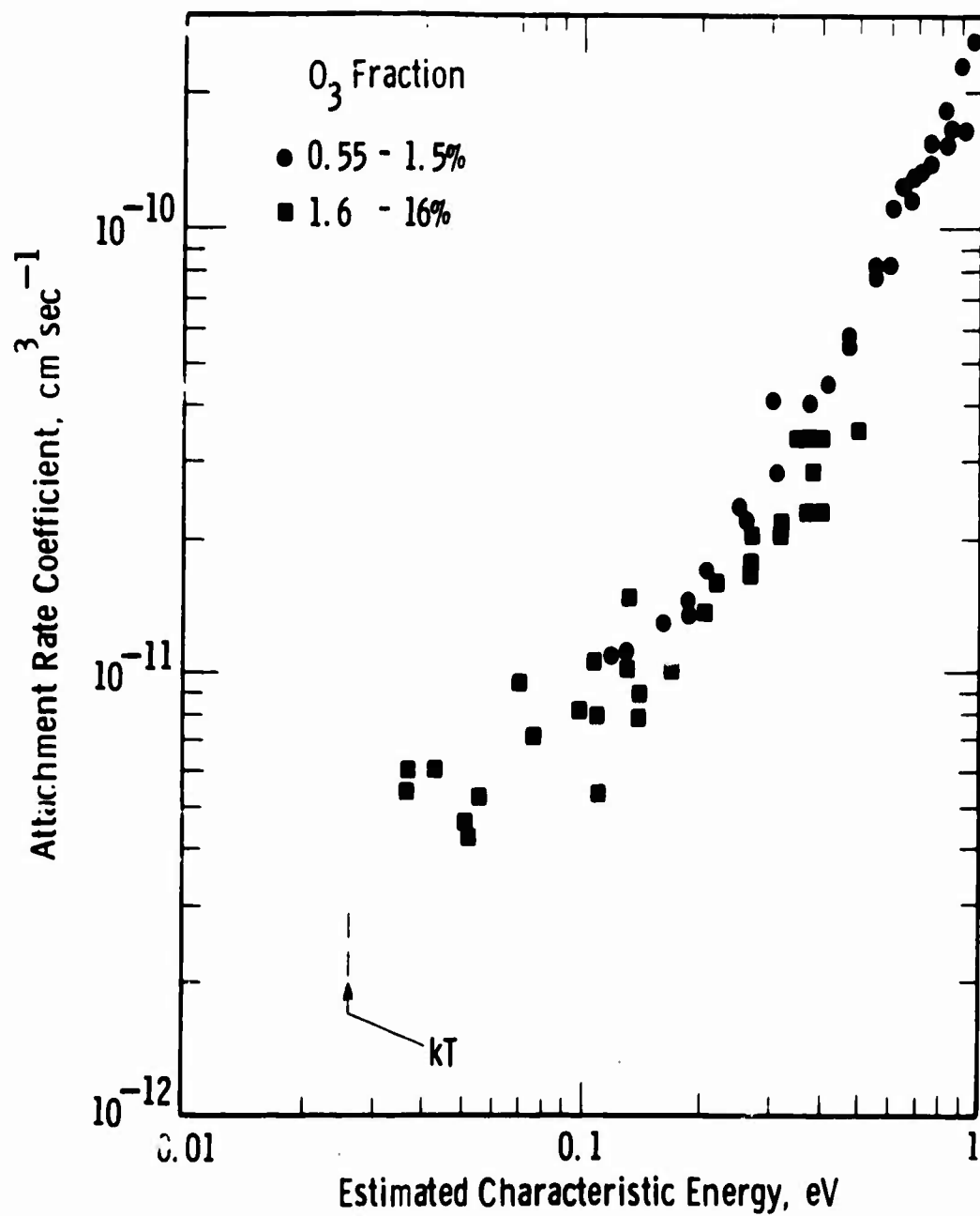
Fig. 7 - Summary of attachment rate coefficient data from measurements in O_3-N_2 mixtures.

15

attachment process, presumably dissociative attachment. The attachment rate coefficient decreases rapidly as the electron energy decreases for electron energies between 1 and 0.1 eV. Unfortunately, there are some questions concerning the interpretation of the data at energies below 0.1 eV. In order to make measurements at these low energies, it is necessary to use large amounts of ozone and high nitrogen pressures. Under these conditions, it is possible that a three-body attachment reaction to normal oxygen, using nitrogen (Ref. 9) as a third body, might occur. Normal oxygen can be present in the system because it is produced when ozone is destroyed on the surfaces. It is also possible that some oxygen might be trapped along with the ozone in the cold trap. Preliminary indications are that this effect is small. Another possible source of error at low energies is that the calculated energy scale may be incorrect. Further work is necessary to clarify the low-energy situation.

5. Discussion

The data presented in Figure 7 indicate that a rapid two-body attachment process occurs in ozone. The attachment rate coefficient is approximately 7×10^{-12} cm^3 sec^{-1} at 0.08 eV and increases to 3×10^{-10} cm^3 sec^{-1} at 1 eV. This is in fair agreement with the results of Curran (Ref. 12) who found both O^- and O_2^- ions formed in ozone at electron energies between 0 and 3 eV. The reactions Curran postulated are

$$O_3 + e \rightarrow O^- + O_2 \tag{5}$$

and

$$O_3 + e \rightarrow O_2^- + O \tag{6}$$

On the basis of Curran's data and the data presented in this paper, reaction (5) appears to have a threshold at near-zero electron energy.

16

Curran found a threshold of about 0.4 eV for reaction (6). However, if one uses our value (Ref. 9) of 0.43 eV for the electron affinity of O_2, the threshold must be nearer 0.6 eV. In any case, it would appear that the primary negative ion formed in the present experiments is O^-.

Recent data by Fehsenfeld, Schemltekopf, and Ferguson (Ref. 2) have shown that both O^- and O_2^- react with O_3 in the following manner;

$$O^- + O_3 \rightarrow O_3^- + O \qquad (7)$$

and

$$O_2^- + O_3 \rightarrow O_3^- + O_2 \qquad (8)$$

with rate coefficients of 7×10^{-10} and 3×10^{-10} cm^3 sec^{-1}, respectively. At the ozone pressures used in these experiments the lifetime of O^- or O_2^- would thus be less than 10^{-5} sec. It thus appears possible that the detachment reaction observed at lower ozone pressures might be,

$$O_3^- + O_3 \rightarrow 3O_2 + e \qquad (9)$$

Unfortunately, we have no direct evidence that O_3^- is the ion that undergoes associative detachment. Experiments show that in many gases (Ref. 13) complex clustering can occur at the pressures used in the present experiments, so that small amounts of impurities, CO_2, for example, can change the identity of the ions. Until mass identification of the negative ions involved is carried out, it is impossible to arrive at any reliable conclusions concerning the details of the reaction scheme occurring in ozone.

In view of the large scatter in the experimental data of Figure 7 at low-electron energies, any attachment coefficient derived by extrapolation to thermal energies (300°K or 0.026 eV) is very uncertain; thus, we suggest a value between 10^{-12} and 10^{-11} cm^3 sec^{-1}

17

or $3 \times 10^{-12\pm0.5}$ cm^3 sec^{-1}. These values are roughly an order of magnitude larger than the rate coefficient obtained by Knapp and Fisher (Ref. 1) and may be sufficiently large to make up for the apparently large values (Ref. 14) of ozone concentration used by Knapp and Fisher. Our estimated thermal attachment coefficient for electrons in O_3 is approximately an order of magnitude smaller than the estimate given by Fehsenfeld et al. (Ref. 2). This ratio is consistent with the suggestion by these authors that the mean energies of their electrons were significantly above thermal.

SECTION III

ELECTRON-ION RECOMBINATION IN ATMOSPHERIC GASES

1. Introduction

One of the principal ionospheric positive ions in the altitude range of 75 to ≈ 200 km has been shown (Ref. 15) to be O_2^+. Analyses (Ref. 16) of the relevant atomic collision reactions indicate that the rate of removal of electrons from this region is to a large extent controlled by dissociative recombination of the electrons with O_2^+ ions. Therefore, we have undertaken extensive afterglow studies of the recombination coefficient for electrons with O_2^+ ions over the temperature range of 205 to 690°K. These studies are somewhat more difficult than the related N_2^+ measurements (Ref. 17 and 18), in that problems arise in producing a plasma with O_2^+ ions in their ground electronic state and in avoiding negative ion accumulation, with attendant effects on the afterglow decay.

In this section of the report, we describe the modifications of the afterglow measuring technique required for the oxygen studies and discuss the atomic collision processes leading to production of O_2^+ ions in their ground electronic state. We then analyze the measurements to obtain the temperature dependence of the coefficient $\alpha(O_2^+)$ for the recombination of electrons and O_2^+ ions, and to obtain an approximate value of the coefficient $\alpha(O_4^+)$ for the recombination of electrons and O_4^+ ions.

2. Experimental Method

The apparatus used in these experiments combines microwave techniques for determining average electron densities during the afterglow of a pulsed discharge with a differentially pumped mass spectrometer that samples the ions diffusing to the wall of the microwave cavity. Inasmuch as most of the apparatus has been described in detail in previous papers (Ref. 17,18) and technical reports (Ref. 19,20), we shall elaborate on only those additional features required for the oxygen study.

19

The microwave cavity and mass spectrometer are shown schematically in Figure 8. In the operation of the microwave system (see Figure 1 of Ref. 17) a pulse from a magnetron ($\approx$2 msec duration) is used to ionize the gas in the cavity. A low-energy probing-microwave signal is used to determine the resonant frequency of the cavity at successive times during the afterglow, from which the average electron density at each of these times can be calculated.

In order to avoid negative ion accumulation from one discharge-afterglow cycle to the next, the apparatus is operated in a "single pulse-afterglow" mode in which the plasma is permitted to decay for approximately 10 sec between cycles. Reproducible plasma generation from cycle to cycle is assured by providing initiating electrons from a pulsed electrode (see Figure 8) to which is applied a 1 kV, 50 μsec impulse at the beginning of each discharge.

The differentially pumped mass spectrometer shown in Figure 8 samples ions diffusing to the cavity wall and effusing through a small orifice, as in the earlier studies of nitrogen (Ref. 17,18). With the "single pulse-afterglow" technique, the signals are correspondingly smaller than in the nitrogen work, where the discharge-afterglow cycle was repeated some 40 times per second. We have, therefore, employed a signal accumulation technique to obtain accurate measurements of the ion decay during the afterglow. To this end, the afterglow is divided into 100 equal time intervals of 300 to 600 μsec duration. The voltage pulses resulting from the transit of single ions through the mass spectrometer/secondary electron multiplier (see Figure 8) are fed through an amplifier and discriminator into a multichannel analyzer.[*] As the multichannel analyzer advances from channel to channel the numbers of ions counted in the corresponding time intervals in the afterglow are recorded in the memory section. By accumulating the afterglow ion counts for 100-1000 "single pulse-afterglow" cycles, statistical fluctuations in the data are reduced to low levels (<10 percent).

---

[*] Technical Measurement Corporation Model 400 C.

20
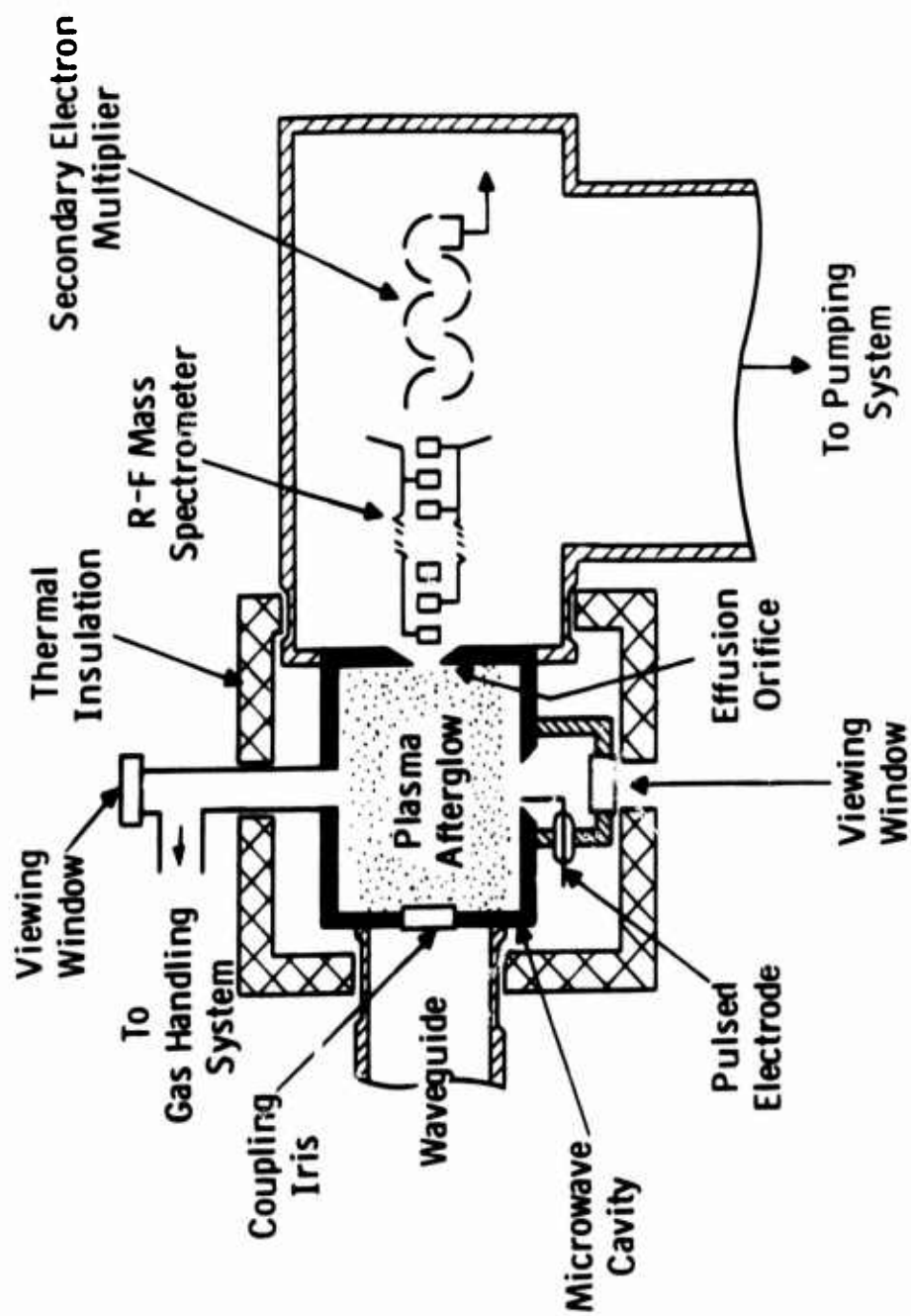
Fig. 8 – Microwave afterglow apparatus showing the microwave cavity and the radio-frequency mass spectrometer.

21

3. Relevant Afterglow Processes

In order to simplify the analysis of the afterglow suffi-
ciently to yield quantitative determinations of the recombination co-
efficient $\alpha(O_2^+)$ it is necessary to achieve conditions in which O_2^+
is the only significant afterglow ion and electron-ion recombination
dominates the volume loss of electrons. The formation of complex ions,
e.g., O_3^+ and O_4^+, is reduced by use of small concentrations of O_2
molecules $[p(O_2) \sim 10^{-3}$ Torr$]$ with the addition of an "inert" neon
buffer gas $[p(Ne) \sim 20$ Torr$]$ to inhibit diffusion to the walls. In
such a mixture one of the dominant production mechanisms for O_2^+ is
the Penning reaction

$$Ne^M + O_2 \rightarrow Ne + O_2^+ + e, \tag{10}$$
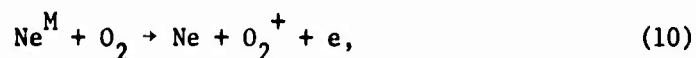
where the superscript M indicates a metastable excited state. Unfor-
tunately, in this reaction there is sufficient excitation energy to
create the ions not only in the desired ground electronic state $X\,{}^2\Pi_g$
but also in the excited electronic state $a\,{}^4\Pi_u$. For this reason, we
have used triple mixtures, adding approximately 1 Torr of Ar, or Kr,
to the O_2 - Ne mixtures in an attempt to produce O_2^+ ions in only the
$X\,{}^2\Pi_g$ state. Assuming comparable cross sections for the Penning ioniza-
tion of O_2 and Ar, or Kr, by neon metastable atoms and using the rele-
vant charge transfer cross sections (Ref. 21) it appears that the pro-
bable ion production sequence in the triple gas mixtures involves
Penning ionization of Ar (or Kr) by the neon metastable atoms followed
by charge transfer of the resulting Ar^+ (or Kr^+) ions with O_2 to form
O_2^+. In the Kr^+ charge transfer reaction the available energy is not
sufficient to excite the O_2^+ ions beyond the $v = 8$ vibrational level
of the ground electronic state.

A second reason for using as small a neutral O_2 density as
practicable is to avoid appreciable negative ion formation during
either the discharge or the afterglow. It has been shown (Ref. 22,23)
that the electron ambipolar diffusion loss rate increases in proportion

22

to the negative ion-electron concentration ratio. In addition, positive ion-negative ion recombination must be considered if this ratio is not small compared to unity. Use of the "single pulse-afterglow" technique mentioned earlier is dictated by the fact that, even if the negative ion production by electron attachment is small in a given discharge-afterglow cycle, the negative ions are essentially trapped in the plasma (Ref. 22,23) and their concentration will build up unless sufficient time elapses between cycles to permit the plasma to decay completely.

Having chosen conditions in which O_2^+ in the desired state is the only significant positive ion, negative ions being essentially absent, and electron-ion recombination is the principal electron loss process, we may approximate the electron continuity equation during the afterglow by

$$\partial n_e / \partial t = -\alpha n_e^2 + D_a \nabla^2 n_e \tag{11}$$

where α and D_a are the recombination and ambipolar diffusion coefficients, respectively. We have invoked the quasineutrality of a plasma to set $n_+ \approx n_e$. In spite of the fact that volume recombination greatly outweighs ambipolar diffusion in determining the electron loss rate, the diffusion term has been included, inasmuch as it has a pronounced effect on the spatial distribution of the electrons within the microwave cavity.

Computer solutions of Eq. (11) subject to the boundary condition $n_+ = n_e \approx 0$ at the walls of the cavity (Ref. 24,25) permit us to obtain quantitative determinations of α from the measured rates of decay of the average electron density during the afterglow. The particular average used in the present analysis, the so-called "microwave-average" electron density, is defined by

$$\bar{n}_{\mu w}(t) \equiv \int_V n_e(\vec{r},t) E^2(\vec{r}) dV \bigg/ \int_V E^2(\vec{r}) dV = \Delta f(t)/C \tag{12}$$

23

where $E(\vec{r})$ is the electric field of the microwave probing signal. The integration extends over the volume of the cavity. This average has the virtue that its value does not depend upon assumptions concerning the form of the electron distribution within the cavity; it is simply equal to the measured cavity frequency shift $\Delta f(t)$, divided by a group of physical constants C (Ref. 26). In addition, in the present case, where the plasma fills the entire cavity volume, $\bar{n}_{\mu w}(t)$ has the same value as the electron density obtained from $\Delta f(t)$ on the artificial assumption that the electrons are uniformly distributed throughout the volume. [This assumption has been widely used previously (Ref. 27).]

The elementary "recombination solution" of Eq. (11) which results when the diffusion term is neglected is

$$1/\bar{n}_{\mu w}(t) = 1/\bar{n}_{\mu w}(0) + t. \tag{13}$$

In many cases it is convenient to plot our data as the reciprocal of $\bar{n}_{\mu w}(t)$ versus afterglow time to display recombination control of the afterglow. Recombination coefficients α may be obtained from the slopes of the straight line sections in these $1/\bar{n}_{\mu w}(t)$ vs. time curves by using appropriate Gray and Kerr correction factors (Ref. 24). Alternately we can obtain α by making a direct comparison of the measured $\bar{n}_{\mu w}(t)$ with the predicted $\bar{n}_{\mu w}(t)$ curves obtained by computer solution (Ref. 25) of Eq. (11) when known values of D_a are inserted and α is treated as a parameter.*

4. Results and Discussion

To insure reliable quantitative measurements of the rate of recombination of O_2^+ ions with electrons, two key requirements should be met. First, the average electron density decay should follow the form given by the computer solution of Eq. (11) for recombination controlled conditions. This, in turn, implies that a linear increase of

---

*L. Frommhold (private communication) has provided computer solutions of Eq.(11) for our experimental conditions.

24

$1/\bar{n}_{\mu w}(t)$ with time [see Eq. (13)] be observed for an appreciable elec-
tron density range. Second, O_2^+ should be the only significant after-
glow ion and its observed wall current (the mass spectrometer output)
should approximately follow the volume electron density decay during
the afterglow. The first condition has been achieved by assuring that
no significant ionization occurs during the afterglow and that the
ambipolar diffusion rate is small. A simple optical absorption system
(Ref. 17) making use of an optical path through the plasma via the
viewing windows (see Figure 8) monitors the neon metastable concentra-
tion. Thus we are able to choose a discharge pulse length that leads
to a sufficiently small metastable density at the start of the after-
glow (Ref. 17) that the rate of Penning ionization, reaction (10), is
negligible. As noted earlier, the ambipolar diffusion to the walls
is made very small by use of a high (≈ 20 Torr) pressure of neon buffer
gas.

The expectation that the O_2^+ wall current should approximately
follow the volume electron density decay arises from the fact that the
computer solution of the positive ion continuity equation (which is
identical to Eq. (11) with n_+ replacing n_e everywhere) indicates that
for much of the afterglow the form of the ion and electron density
distributions within the cavity remains approximately constant [c.f.
Gray and Kerr (Ref. 24)]. Thus the ion diffusion current to the wall,
which is proportional to $(\nabla n_+)_{wall}$, decreases approximately as n_+ (and
hence n_e) decreases in the volume.

An example of the observed electron and ion decays is shown
in Fig. 9 for a binary mixture of oxygen (1.1×10^{-3} Torr) and neon
(20 Torr) at 295°K. It will be seen that $1/\bar{n}_{\mu w}(t)$ increases linearly
with time over a density range, $f \approx 10$, and that after approximately
4 msec the reciprocal of the O_2^+ wall current follows the electron
decay (O_2^+ is the only significant afterglow ion). The solid line
represents the predicted electron density decay obtained from the
computer solution of Eq. (11) with $D_a p = 360$ (cm^2/sec)-Torr for O_2^+
ions in neon (Ref. 28) and a value of $\alpha(O_2^+) = 2.2 \times 10^{-7}$ cm^3/sec.
This computation uses an initial electron and ion distribution that is

25

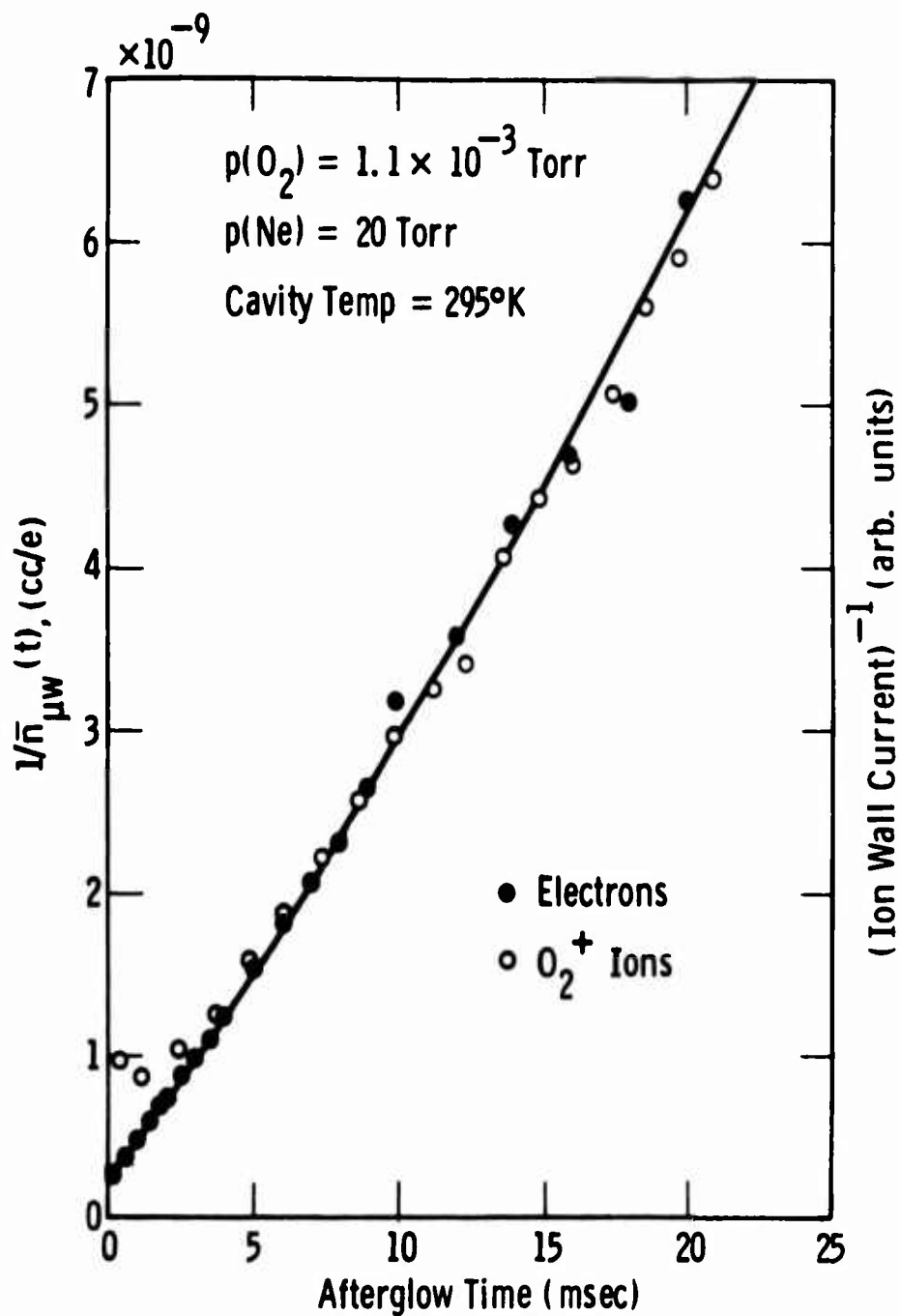Fig. 9 - Reciprocal plots of observed electron density and O_2^+ wall currents as functions of time in the afterglow of an O_2-Ne microwave discharge. The O_2^+ wall currents have been normalized to the electron density at an afterglow time of 6 msec. The solid line represents a numerically computed fit to the observed electron density, taking into account both the recombination and ambipolar diffusion loss mechanisms.

a fundamental mode diffusion distribution, reasonably approximating the actual starting distribution created by the microwave discharge. In addition, after ≤ 1 ms the predicted decays are rather insensitive to the starting distribution (Ref. 25,29) unless extreme forms, such as highly constricted plasmas, are used.

It is interesting to note that if the measured slope of Figure 9 is corrected using the Gray and Kerr correction factors (Ref. 24) corresponding to a spherical plasma container having a fundamental diffusion length, $\Lambda = 1.125$ cm, equal to that of our rectangular parallelepiped cavity, a value $\alpha(O_2^+) = 2.1 \times 10^{-7}$ cm^3/sec is obtained. This result is in good agreement with the value obtained by computer solution for the rectangular geometry. Therefore, for most of the experimental data, we have obtained corrected values of the recombination coefficient by applying Gray and Kerr correction factors in the above manner, rather than by obtaining computer solutions for each decay curve.

In the early phases of this study, binary O_2-Ne mixtures were used for the recombination measurements. When "single pulse-afterglow" techniques were employed, linear $1/\bar{n}_{\mu w}(t)$ vs time curves were obtained with satisfactory tracking of the electron density and O_2^+ wall current decays. However, unlike the recombination studies in nitrogen (Ref. 17,18), where the values of $\alpha(N_2^+)$ did not depend on the N_2 partial pressure, the coefficient $\alpha(O_2^+)$ varied significantly with the partial pressure of O_2 used, as is shown by the short-dashed curve of Figure 10.

A possible explanation of the observed variation in $\alpha(O_2^+)$ with O_2 pressure in the binary mixtures lies in the fact, noted in Sect. III-3, that more than one electronic state of O_2^+ can be formed in the Penning reaction. In an effort to avoid formation of electronically excited O_2^+ ions, we first added approximately 1 Torr of Ar, then of Kr, to the binary gas mixture. Under these conditions one hopes to excite the X $^2\Pi_g$ state of O_2^+ by the sequence Ne$^M \rightarrow$ Ar$^+$ (or Kr$^+$) $\rightarrow O_2^+$. Unfortunately, when Ar is added to the binary mixture, the energetics of the charge transfer reaction from Ar$^+$ still permit excitation of many (v > 20) vibrational levels of the X $^2\Pi_g$ state of
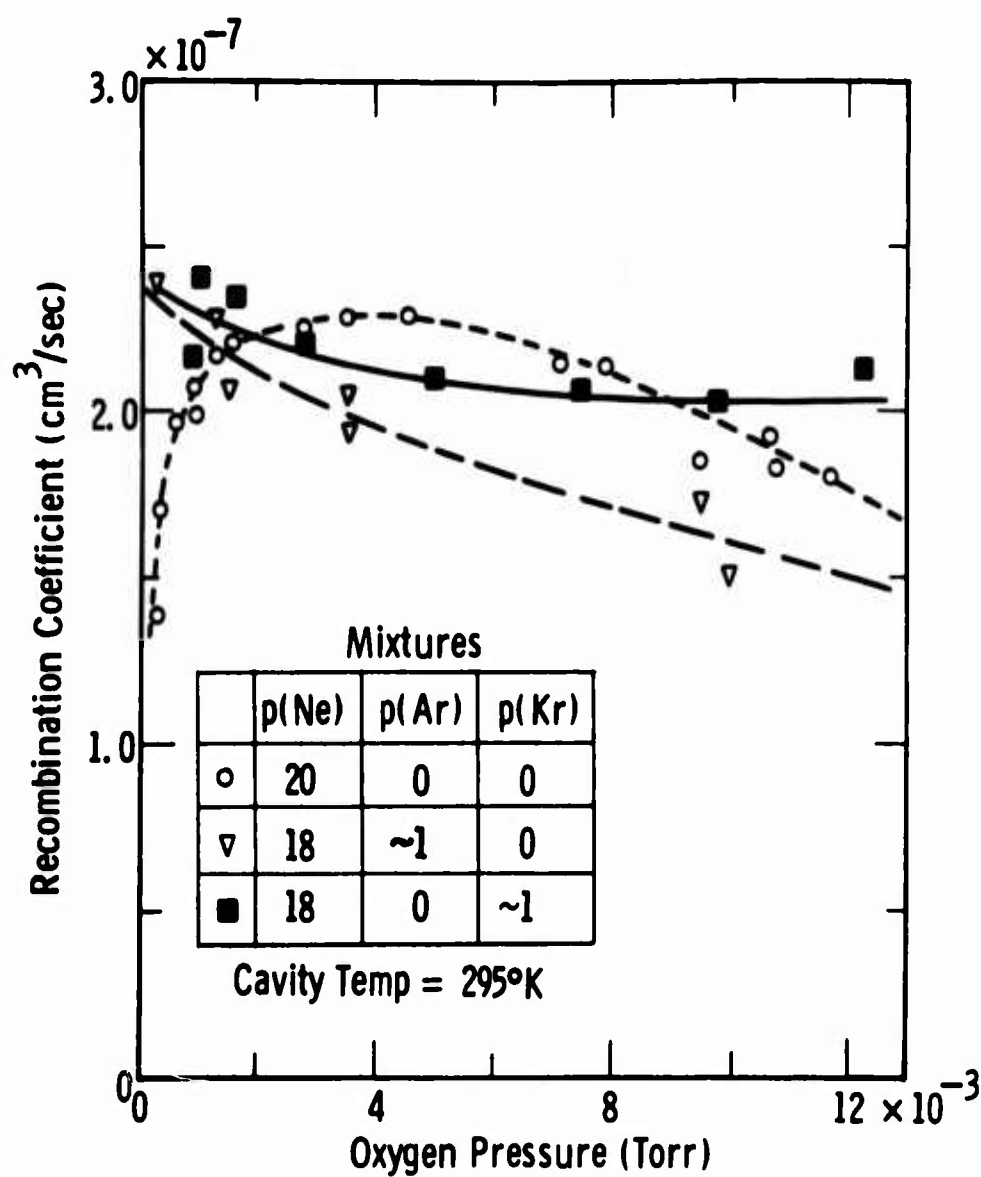
27

Fig. 10 - Observed oxygen pressure dependence of the recombination
coefficient $\alpha(O_2^+)$. The short dashed, long dashed, and
solid lines correspond to O_2-Ne, O_2-Ne-Ar, and O_2-Ne-Kr
gas mixtures, respectively.

28

O_2^+, and, as indicated by the long-dashed line in Figure 10, also yields a significant variation of $\alpha(O_2^+)$ with changing oxygen pressure. When Kr was added to the O_2-Ne mixture, a much weaker dependence of $\alpha(O_2^+)$ on oxygen pressure was noted (solid curve of Figure 10). Here, only the lower vibrational levels ($v \leqslant 8$) of the O_2^+ ground electronic state can be excited in the charge transfer from Kr^+. In the discussion of the temperature dependence measurements which follow, we have included data obtained in O_2-Ne and O_2-Ne-Kr mixtures. The observed recombination coefficients obtained using O_2-Ne-Kr mixtures show no significant dependence on the oxygen pressure except at the lowest temperature investigated (205°K). The O_2 densities (3.5 x 10^{13} to 2.5 x 10^{14} cm^{-3}) used in obtaining experimental data in O_2-Ne mixtures correspond to the O_2 pressure range (1 x 10^{-3} to 8 x 10^{-3} Torr) in Figure 10 over which $\alpha(O_2^+)$ shows the least variation. In no case have we observed a significant dependence of $\alpha(O_2^+)$ on the pressure of neon buffer gas.

In order to obtain values of $\alpha(O_2^+)$ at temperatures above and below 295°K, the cavity has been thermally isolated from the rest of the apparatus (Ref. 18) and either a heater or a refrigerating bath placed inside of the thermal insulation shown in Figure 8. At temperatures above approximately 500°K significant concentrations of impurity ions, resulting, presumably, from thermal desorption from the cavity walls, are observed in the mass spectra. By means of an auxiliary pumping line attached to the cavity (not shown in Figure 8) it has been possible to significantly increase the gas flow rate and effectively reduce the impurity concentration, thereby permitting operation at higher temperatures. In this way afterglow measurements have been obtained over the temperature range 205 to 690°K.

The results of the measurements of the temperature dependence of $\alpha(O_2^+)$ are shown by the solid data points in the log-log plot of Figure 11, the triangular points indicate the O_2-Ne mixture results, while the solid circles indicate the O_2-Ne-Kr mixture results. In nearly all cases these data points represent the average of several
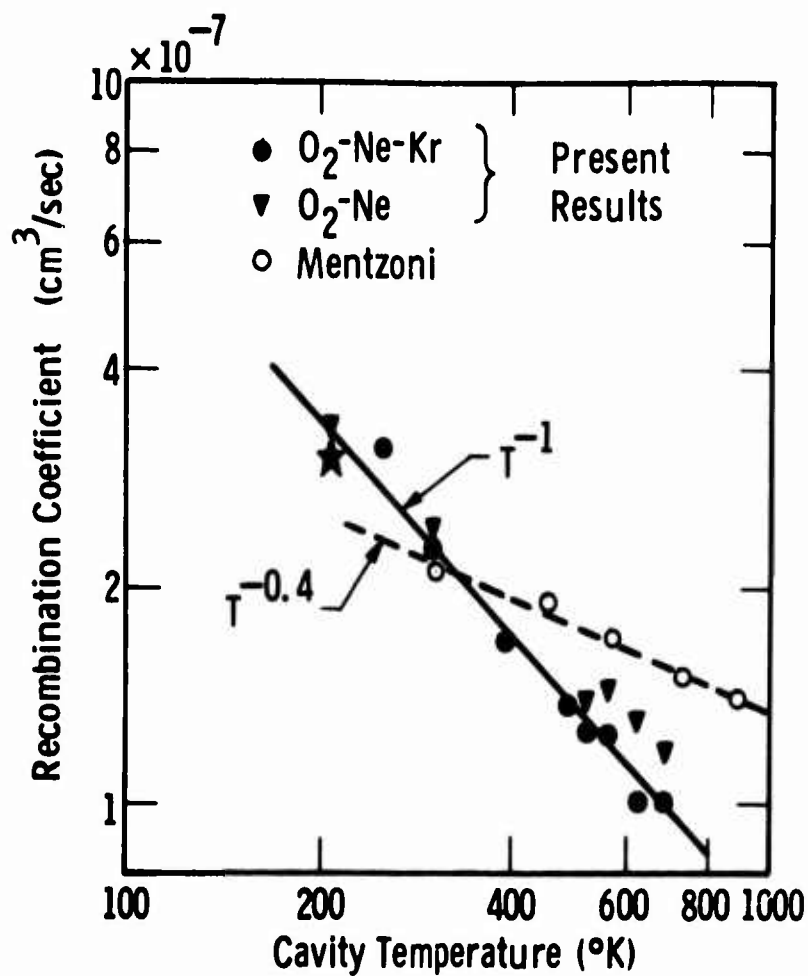
29

Fig. 11 – Observed temperature dependence of the coefficient for the recombination of O_2^+ ions and electrons obtained from after-glow studies in O_2-Ne and O_2-Ne-Kr gas mixtures. The single point (★) is a derived value of $\alpha(O_2^+)$ obtained under conditions where O_4^+ was a significant afterglow ion (see text and Fig. 12).

measurements of $\alpha(O_2^+)$ at the respective temperatures. The single
point (★), corresponding to a temperature of 205°K, is a derived value
for $\alpha(O_2^+)$ obtained under conditions where O_4^+ was a significant after-
glow ion. The method of obtaining $\alpha(O_2^+)$ in this case will be discussed
in more detail below. In most of the experimental data presented in
Figure 11, we observed similar decay rates for the electron density
and O_2^+ wall currents. The exceptions occurred at 205°K, where signi-
ficant O_4^+ concentrations were observed, and at the highest temperature,
~690°K. There is no apparent explanation for the observed discrepancy
in the decay rates at the high temperatures.

For purposes of comparison, we have also included in Figure
11 the results obtained by Mentzoni (Ref. 30) for unidentified ions in
oxygen. One notes that at room temperature (≈295°K) the present results
are in good agreement with those of Mentzoni. However, the observed
temperature dependence, which is reasonable well represented by the
relation $\alpha(O_2^+) \propto T^{-1}$ (the solid line), is significantly stronger than
indicated by Mentzoni's data (the dashed line).

It has been noted that the measured recombination coefficients
obtained at low temperatures (205°K) from O_2-Ne-Kr mixtures exhibit a
significant dependence on the oxygen pressure. In addition, the ob-
served recombination coefficients seem unusually large, the values
ranging from 8.0×10^{-7} cm^3/sec to 2.5×10^{-6} cm^3/sec. The corres-
ponding values of $\alpha(O_2^+)$ obtained from O_2-Ne mixtures is 3.3×10^{-7}
cm^3/sec (see Figure 11). Mass spectrometer studies indicate that the
abnormal behavior observed in O_2-Ne-Kr mixtures at the low temperatures
is related to the appearance of O_4^+ as a significant afterglow ion.
In this case the observed decay rates of the O_4^+ and O_2^+ ions are quite
similar, suggesting an essentially constant $[O_4^+]/[O_2^+]$ concentration
ratio during the afterglow, and hence, a thermodynamic equilibrium
behavior.

If such an equilibrium behavior does exist it is a simple
matter to show that the electron density decay will follow Eq. (13)
with an effective recombination coefficient, α_{eff}, given by

31

$$\alpha_{eff} = (R_o \alpha_4 + \alpha_2)/(R_o + 1) \tag{14}$$

where $\alpha_4 = \alpha(O_4{}^+)$, $\alpha_2 = \alpha(O_2{}^+)$, and R_o is the time independent ratio of $[O_4{}^+]/[O_2{}^+]$ ion densities within the cavity. From this expression we note that a plot of $\alpha_{eff}(R_o + 1)$ versus R_o should yield a straight line having a slope α_4 and an intercept α_2. This predicted behavior is not followed if we assume that the measured ion current ratio F is an accurate representation of the ion density ratio R_o. In the present experiment it is quite possible that discrimination against the weakly bound $O_4{}^+$ ions takes place in drawing the ions from the microwave cavity as a result of breakup collision in the ion accelerating region, in which case, $R_o > R$. By using our measured oxygen pressure data and extrapolating the $O_4{}^+$-$O_2{}^+$ equilibrium constant obtained by Yang and Conway (Ref. 31) to our temperature (205°K), we find that the computed $[O_4{}^+]/[O_2{}^+]$ density ratio in the cavity is approximately 5.5 times larger than the corresponding measured $O_4{}^+/O_2{}^+$ ion wall current ratio. The data presented in Figure 12 is based on this relation, $R_o = 5.5$ R. In this case a straight line dependence on R_o is obtained, the slope and intercept of the line yielding recombination coefficients $\alpha(O_4{}^+) \doteq 2.3 \times 10^{-6}$ cm^3/sec and $\alpha(O_2{}^+) \doteq 3 \times 10^{-7}$ cm^3/sec, respectively.

Thus, it appears that the anomalous behavior at low temperatures can indeed be explained by the fact that the weakly bound $O_4{}^+$ ions, which have a large recombination coefficient, become increasingly more important at low temperatures.

5. Conclusions

From the foregoing discussion we conclude that the values of $\alpha(O_2{}^+)$ for $O_2{}^+$ ions in the $X\ ^2\Pi_g$ ground electronic state vary from $(3.0 \pm 0.3) \times 10^{-7}$ cm^3/sec at $T_e = T_+ = T_{gas} = 205°K$ to $(1.0 \pm 0.2) \times 10^{-7}$ cm^3/sec at 690°K (see Figure 11). As a result of the mode of ion formation, it is energetically possible that the $O_2{}^+$ ions are created in an excited vibrational state ($v \le 8$). However, inasmuch as the

32
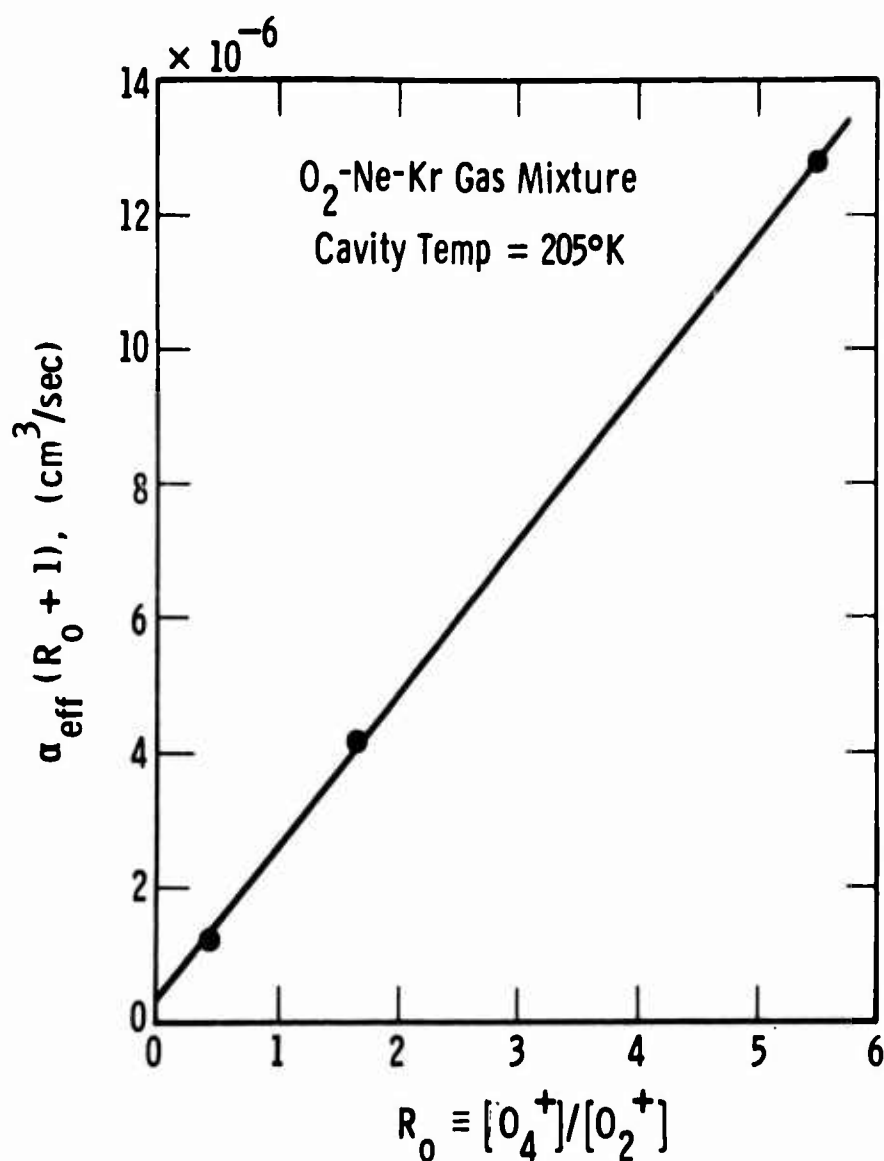
Fig. 12 – Dependence of the effective recombination coefficient α_{eff} on the $[O_4^+]/[O_2^+]$ concentration ratio R_o. α_{eff} has been multiplied by the factor (R_o+1) in order to show the fit of the experimental data to Eq. (14). The slope and intercept of the solid line yield recombination coefficients $\alpha_4 \cong$ 2.3×10^{-6} cm^3/sec and $\alpha_2 \cong 3 \times 10^{-7}$ cm^3/sec, respectively.

33

recombination loss is studied over some 10 msec of the afterglow, there may be time for the initial vibrational excitation to decay via vibration exchange collisions* with O_2 molecules of the type $(v, 0) \rightarrow (v-1, 1)$ before recombination occurs. Thus, the present values of $\alpha(O_2^+)$ probably refer to ions in the same state as are produced in the ionosphere by photoionization and are, therefore, appropriate for use in ionospheric model calculations.

The analysis of the contribution of O_4^+ ions to the recombination loss at 205°K leads to an approximate value $\alpha(O_4^+) = 2.3 \times 10^{-6}$ cm^3/sec. It is interesting to note that this value is about the same order of magnitude as that obtained (Ref. 17) for N_4^+ $[\alpha(N_4^+) = 2 \times 10^{-6}$ cm^3/sec at 300°K] and for the dimer ion $NO \cdot NO^+$ (Ref. 32). Thus, it appears that the dimer ions, $O_2 \cdot O_2^+$, $N_2 \cdot N_2^+$, and $NO \cdot NO^+$ all exhibit substantially larger recombination coefficients than the corresponding monomer ions.

---

*Calculations of the vibrational relaxation of O_2^+ ions in O_2 [see, for example, H. Skin, Ion-Molecule Reactions in the Gas Phase, edited by P. J. Ausloos (American Chemical Society Publications, Washington, D. C., 1966) p. 44] indicate that the vibrational relaxation time for the process $(1,0) \rightarrow (0,0)$ is ~1 to 10 sec in our experiments. We would expect the vibrational relaxation times for exchange collisions of the type $(v,0) \rightarrow (v-1,1)$ between O_2^+ ions and O_2 molecules to be much shorter since the vibrational spacing of the ion and molecule are comparable and; hence, there is very little transfer of potential energy into kinetic energy.

REFERENCES

1. W. S. Knapp and P. G. Fisher, "Atmospheric Deionization Models Inferred from Nuclear Burst Environments", DASA Symposium on Physics and Chemistry of the Lower Ionosphere, Boulder, Colorado, June 1965.

2. F. C. Fehsenfeld, A. L. Schmeltekopf, H. I. Schiff and E. E. Ferguson, "Laboratory Measurements of Negative Ion Reactions of Atmospheric Interest", Planet. Space Sci. 15, 373 (1967); and E. E. Ferguson, "Ionospheric Ion-Molecule Reaction Rates", Rev. of Geophys. 5, 305 (1967).

3. A. Mathias and H. I. Schiff, "Role of Excited Molecules in a Stream of Electrically Charged Oxygen", J. Chem. Phys. 10, 3118 (1964).

4. D. Alpert, C. G. Matland and A. O. McCoubrey, "A Null Reading Absolute Manometer", Rev. Sci. Insts. 22, 370 (1951).

5. E. C. Y. Inn and Y. Tanaka, "Ozone Absorption Coefficients in the Visible and Ultraviolet Region", Ozone Chemistry and Technology, (Am. Chem. Soc., Washington, 1959), page 263.

6. J. L. Moruzzi, "A Simple High Emission Photocathode", Rev. Sci. Insts. 38, 1284 (1967).

7. L. B. Loeb, Basic Processes in Gaseous Electronics, (University of California Press, Berkeley, California, 1955), Chapter 5.

8. L. M. Chanin, A. V. Phelps and M. A. Biondi, "Measurements of the Attachment of Low Energy Electrons to Oxygen Molecules", Phys. Rev. 128, 219 (1962).

9. J. L. Pack and A. V. Phelps, "Electron Attachment and Detachment I-- Pure O_2 at Low Energy", J. Chem. Phys. 44, 1870 (1966).

10. L. S. Frost and A. V. Phelps, "Rotational Excitation and Momentum Transfer Cross Sections for Electrons in H_2 and N_2 from Transport Coefficients", Phys. Rev. 127, 1621 (1962).

11. A. G. Engelhardt, A. V. Phelps and C. G. Risk, "Determination of Momentum Transfer and Inelastic Collision Cross Sections for Electrons in Nitrogen Using Transport Coefficients", Phys. Rev. 135, A1566 (1964).

12. R. K. Curran, "Negative Ion Formation in Ozone", J. Chem. Phys. 35, 1849 (1961).

13. J. L. Moruzzi and A. V. Phelps, "Survey of Negative Ion-Molecule Reactions in O_2, CO_2, H_2O, CO, and Mixtures of the Gases at High Pressure", J. Chem. Phys. 45, 4617 (1966).

14. B. G. Hunt, "Photochemistry of Ozone in a Moist Atmosphere", J. Geophysical Res. 71, 1385 (1966); and J. E. Blamont and T. M. Donahue, "Sodium Dayglow: Observation and interpretation of a Large Diurnal Variation", J. Geophysical Res. 69, 4093 (1964).

15. See, for example, R. S. Narcisi and A. D. Bailey, "Mass Spectrometric Measurement of Positive Ions at Altitudes from 64 to 112 km", J. Geophys. Res. 70, 3687 (1965); and R. C. Whitten and I. G. Poppoff, Physics of the Lower Ionosphere, (Prentice-Hall, Inc., Englewood Cliffs, N. J.).

16. See, for example, T. M. Donahue, "Ionospheric Reaction Rates in the Light of Recent Measurements in the Ionosphere and the Laboratory", Planet. Space Sci. 14, 33 (1966); E. E. Ferguson, et al., "Positive Ion-Neutral Reactions in the Ionosphere", J. Geophys. Res. 70, 4323 (1965); and E. E. Ferguson, "Ionospheric Ion-Molecule Reaction Rates", Rev. of Geophys. 5, 305 (1967).

17. W. H. Kasner and M. A. Biondi, "Electron Ion Recombination in Nitrogen", Phys. Rev. 137, A317 (1965).

18. W. H. Kasner, "Study of the Temperature Dependence of Electron-Ion Recombination in Nitrogen", Phys. Rev. 164, 194 (1967).

19. A. V. Phelps and W. H. Kasner, "Studies and Experimental Work on Atomic Collision Processes Occurring in Atmospheric Gases", Tech. Rept. No. AFWL-TR-66-34, Air Force Weapons Laboratory, Kirtland AFB, N. M., May 1966.

20. A. V. Phelps and W. H. Kasner, "Studies and Experimental Work on Atomic Collision Processes Occurring in Atmospheric Gases", Tech. Rept. No. AFWL-TR-66-121, Air Force Weapons Laboratory, Kirtland AFB, N. M., June 1967.

21. See, for example, P. D. Golden, et al., "Thermal Energy Ion-Neutral Reaction Rates. II. Some Reactions of Ionospheric Interest", J. Chem. Phys. 44, 4095 (1966); F. C. Fehsenfeld, et al., "Thermal Energy Ion-Neutral Reaction Rates. VI. Some Ar^+ Charge Transfer Reactions", J. Chem. Phys. 45, 404 (1966).

22. M. A. Biondi, "Dissociative Attachment of Electrons in Iodine I. Microwave Determination of the Absolute Cross Section at 300°K", Phys. Rev. 109, 2005 (1958).

23. H. J. Oskam, "Microwave Investigation of Disintegrating Gaseous Discharge Plasmas", Phillips Res. Rept. 13, 401 (1958).

24. E. P. Gray and D. E. Kerr, "The Diffusion Equation with a Quadratic Loss Term Applied to Electron-Ion Volume Recombination in a Plasma", Ann. Phys. (N.Y.) 17, 276 (1962).

25. L. Frommhold and M. A. Biondi, "A Mathematical Study of the Electron Decay in Diffusion and Recombination Controlled Afterglows", submitted to Annals of Physics.

26. See, for example, M. A. Biondi, "Measurement of the Electron Density in Ionized Gases by Microwave Techniques", Rev. Sci. Instr. 22, 500 (1951).

27. See, for example, M. A. Biondi and S. C. Brown, "Measurement of Electron-Ion Recombination", Phys. Rev. 7 , 1697 (1949).

28. W. H. Kasner, W. A. Rogers, and M. A. Biondi, "Electron-Ion Recombination Coefficients in Nitrogen and Oxygen", Phys. Rev. Letters 7, 321 (1961). See also, Fig. 6 of L. M. Chanin and M. A. Biondi, "Mobilities of Mercury Ions in Helium, Neon, and Argon", Phys. Rev. 107, 1219 (1957).

29. L. Frommhold, M. A. Biondi and J. Mehr, "Electron Temperature Dependence of Electron-Ion Recombination in Neon", Phys. Rev. 165, 44 (1968).

30. M. H. Mentzoni, "Electron Removal During the Early Oxygen Afterglow", J. Appl. Phys. 36, 57 (1965).

31. J. H. Yang and D. C. Conway, "Bonding in Ion Clusters. I. O_4^+", J. Chem. Phys. 40, 1729 (1964).

32. C. S. Weller and M. A. Biondi, "Temperature Dependence of Recombination of NO^+ Ions and Electrons", Bull. Am. Phys. Soc. 13, 199 (1968) and Phys. Rev., to be published.

DOCUMENT CONTROL DATA · R & D

(Security classification of title, body of abstract and indexing annotation must be entered when the overall report is classified)

1. ORIGINATING ACTIVITY (Corporate author)	2a. REPORT SECURITY CLASSIFICATION
Westinghouse Research Laboratories Pittsburgh , Pennsylvania	UNCLASSIFIED
	2b. GROUP

3. REPORT TITLE

STUDIES AND EXPERIMENTAL WORK ON ATOMIC COLLISION PROCESSES OCCURRING IN ATMOSPHERIC GASES

4. DESCRIPTIVE NOTES *(Type of report and inclusive dates)*
20 February 1967 to 21 February 1968

5. AUTHOR(S) *(First name, middle initial, last name)*

A. V. Phelps
W. H. Kasner

6. REPORT DATE	7a. TOTAL NO. OF PAGES	7b. NO. OF REFS
September 1968	50	32

8a. CONTRACT OR GRANT NO. F2960167C-0046	9a. ORIGINATOR'S REPORT NUMBER(S)
b. PROJECT NO. 5710	AFWL-TR-68-55
c.	9b. OTHER REPORT NO(S) (Any other numbers that may be assigned this report)
d.	

10. DISTRIBUTION STATEMENT This document is subject to special export controls and each transmittal to foreign governments or foreign nationals may be made only with prior approval of AFWL (WLRT), Kirtland AFB, NM. Distribution is limited because of the technology discussed in the report.

11. SUPPLEMENTARY NOTES	12. SPONSORING MILITARY ACTIVITY AFWL (WLRT) Kirtland AFB, NM 87117

13. ABSTRACT   (Distribution Limitation Statement No. 2)

The rate coefficients for electron attachment to ozone have been measured in N_2-O_3 mixtures and are found to increase from 8×10^{-12} to 1.8×10^{-10} cm^3/sec as the characteristic electron energy increases from 0.1 and 0.8 eV. The dependence of the attachment rate coefficient on the ozone pressure at electron energies near 0.15 eV is consistent with a two-body attachment process, presumably dissociative attachment. The temperature dependence of the recombination coefficient for electrons and O_2^+ can be approximated by T_{gas}^{-1} with the actual values being $(3.0 \pm 0.3) \times 10^{-7}$ cm^3/sec at 205°K, $(2.2 \pm 0.2) \times 10^{-7}$ cm^3/sec at 295°K, and $(1.0 \pm 0.2) \times 10^{-7}$ cm^3/sec at 690°K. The recombination coefficient for electrons and O_4^+ at 205°K is estimated to be 2.3×10^{-6} cm^3/sec.

DD FORM 1473 REPLACES DD FORM 1473, 1 JAN 64, WHICH IS OBSOLETE FOR ARMY USE.

14. KEY WORDS	LINK A		LINK B		LINK C	
	ROLE	WT	ROLE	WT	ROLE	WT
Electron attachment in ozone						
Electron detachment in ozone						
Drift tube experiment						
Electron-ion recombination						
Atmospheric gases						
Afterglow experiment						

AFSC (KAFB NM)